SELF-TURNING SCREW MECHANISM FOR BURYING GEOPHYSICAL SENSORS UNDER REGOLITH

S. Yasuda[(1)], K. Komatsu[(2)], S. Tanaka[(2)]

[(1)]JAXA, 2-1-1 Sengen, Tsukuba, Ibaraki, JAPAN, Email:yasuda.susumu@jaxa.jp
[(2)]JAXA, 3-1-1 Yunodai, Chuo-ku, Sagamihara, Kanagawa JAPAN

ABSTRACT

Methods of installing certain geophysical sensors such as seismometers and heat flow sensors underground are needed for future lunar/planetary exploration. On the Moon, installing such units at depths exceeding several tens of centimeters enables overnight survival without any thermally shielded mechanism.
For this purpose, we proposed a new mechanism named "Self-Turning Screw Mechanism" (STSM), which utilizes the reactive torque of a wheel to drill into regolith.
The STSM consists of a body with a screw-like blade, a wheel located inside the body, a motor to drive the wheel, and a clutch that mechanically connects the wheel and body. Repeated acceleration of the wheel and the mechanical connection of the clutch cause the unidirectional rotation of the STSM body, thereby drilling into the regolith.
This paper presents the concept of the STSM, describes our recent prototype designs, and examines the results of related experiments.

1. INTRODUCTION

Methods of installing certain geophysical sensors such as seismometers and heat flow sensors underground are needed for future unmanned lunar/planetary exploration [1]. On the Moon, installing such units at depths exceeding several tens of centimeters enables overnight survival without any thermally shielded mechanism. Also, burying seismometers under the regolith means they will be mechanically fixed to the surface of the Moon. Several mechanisms had been proposed for this requirement [2] [3], but no practical mechanisms have been developed to date. In 2008, we proposed a new mechanism named "Self-Turning Screw Mechanism" (STSM), which utilizes the reactive torque of a wheel to drill into regolith [4]. We report on the concept and simple analytical model of the STSM, the recent prototype designs and their experiments.

2. BASIC PRINCIPLE AND ANALYTICAL MODEL

2.1. Basic Principle

Fig. 1 is the conceptual figure of STSM, which consists of a cylindrical body, a spiral blade provided on its outer surface, a wheel provided inside the body, and a clutch mechanically connecting the wheel and body. STSM uses repeated acceleration of the wheel and the mechanical connection of the clutch to make the STSM body rotate unidirectionally, thereby drilling into the regolith.

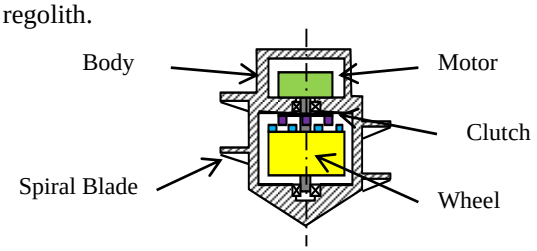

Figure 1. Conceptual figure of STSM

The detailed driving procedure is as follows (Fig. 2):

1. In the initial state, the clutch is free; The body remains against the regolith and the wheel rotates at a certain angular velocity;
2. The clutch is connected, whereupon the wheel decelerates rapidly, the body starts rotating due to reactive torque from the wheel and the spiral blade excavates the regolith;
3. The clutch is released and the wheel gradually accelerated; As the reactive torque from the wheel is less than the frictional torque from the regolith, the body does not rotate;
4. Steps 1 to 3 are repeated.

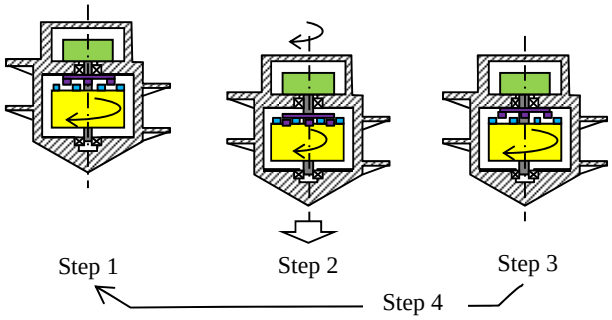

Figure 2. Driving procedure of STSM

STSM has the following features:

(i) a simple, compact, and lightweight self-contained system, needing neither a support structure nor a torque cancelling mechanism such as a contra-rotating screw to resist reactive torque;

(ii) no risk of jamming in the regolith due to the clearance between moving parts, as none are outside the body;
(iii) the capability of digging deeper into the regolith than the length of the STSM itself;
(iv) the capability of driving backward;
(v) relatively low power consumption.

2.2. Analytical Model

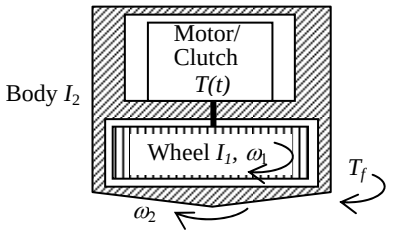

Figure 3. Analytical model of STSM

Fig. 3 depicts a 1-D analytical model of the STSM, which represents rotational movement only. The motor and clutch inside the body generate torque $T(t)$ according to the control signal, while the resistive torque from the regolith T_f works on the outer surface of the body. The equations of motion are as follows;

$$\begin{cases} I_1\dot{\omega}_1 = -T(t) \\ I_2\dot{\omega}_2 = T(t) + T_f \end{cases} \quad (1)$$

I_1, I_2: Moment of inertia (MOI) of the body and the wheel.
ω_1, ω_2: Angular velocity relative to inertial space of the wheel and body.

T_f is the overall resistive torque from the regolith, which includes: the friction between the body and regolith; the force required to excavate the regolith; and the force to move the body forward (or backward). For simplicity, we assume T_f as follows: the direction of T_f is opposite to that of the rotation of the body; the absolute value of T_f is T_{f0}. T_{f0} may differ at each cycle. This is shown in Fig. 4.

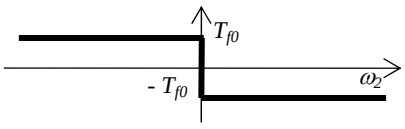

Figure 4. Simplified model of resistive torque from the regolith T_f

We analyze this model according to the driving procedure showed in section 2.1, as follows:

1. $t<0$: $\omega_1 = \omega_0$; $\omega_2 = 0$; $\omega = \omega_2 - \omega_1 = -\omega_0$;
2. $0 \le t \le t_1$: the clutch generates torque and we assume this as constant T_1 for simplicity;
3. $t_1 < t \le t_2$: the wheel and body rotate at same angular velocity, therefore

$$T(t) = \frac{I_1}{I_1 + I_2} T_{f0} \quad (2)$$

4. $t_2 < t \le t_3$: the motor generates constant torque T_2 and the wheel accelerates gradually, while the body is still ($\omega_2 = 0$).

Therefore torque $T(t)$ becomes as follows;

$$T(t) = \begin{cases} 0 & (t < 0) \\ T_1 & (0 \le t \le t_1) \\ \dfrac{I_1}{I_1 + I_2} T_{f0} & (t_1 < t \le t_2) \\ T_2 & (t_2 < t \le t_3) \end{cases} \quad (3)$$

Then, Eq. 1 is solved as follows, and these results are depicted in Fig. 5.

$$\omega_1 = \begin{cases} \omega_0 & (t < 0) \\ -\dfrac{T_1}{I_1} t + \omega_0 & (0 \le t \le t_1) \\ -\dfrac{T_{f0}}{I_1 + I_2} t + \dfrac{I_1}{I_1 + I_2} \omega_0 & (t_1 < t \le t_2) \\ \dfrac{T_2}{I_1}(t - t_2) & (t_2 < t \le t_3) \end{cases} \quad (4)$$

$$\omega_2 = \begin{cases} 0 & (t < 0) \\ \dfrac{T_1 - T_{f0}}{I_2} t & (0 \le t \le t_1) \\ -\dfrac{T_{f0}}{I_1 + I_2} t + \dfrac{I_1}{I_1 + I_2} \omega_0 & (t_1 < t \le t_2) \\ 0 & (t_2 < t \le t_3) \end{cases} \quad (5)$$

$$\begin{cases} t_1 = \left(\dfrac{T_1}{I_1} + \dfrac{T_1 - T_{f0}}{I_2} \right)^{-1} \omega_0 \\ t_2 = \dfrac{I_1}{T_{f0}} \omega_0 \\ t_3 = \left(\dfrac{1}{T_2} + \dfrac{1}{T_{f0}} \right) I_1 \omega_0 \end{cases} \quad (6)$$

Rotation angle of the body θ_2 becomes as follows;

$$\theta_2 = \int_{t=0}^{t=t_2} \omega_2 dt = \frac{I_1^2 \omega_0^2}{2\left(I_1 + \dfrac{T_1}{T_1 - T_{f0}} I_2 \right) T_{f0}} \quad (7)$$

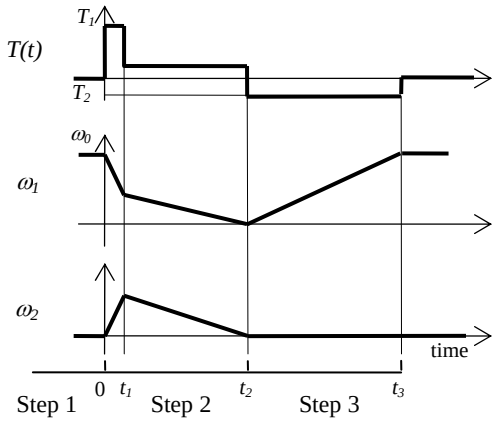

Figure 5. Results of Analysis

From Eq. 7, we learn the following:

1. To increase θ_2, I_1 should be larger and I_2 smaller;
2. θ_2 is proportional to the square of the initial angular velocity of the wheel ω_0 and the inverse of T_{f0}.

Assuming $T_1 \to \infty$, from the law of conservation of angular momentum, the angular velocity of the body and the wheel ω' right after the connection of the clutch becomes as follows;

$$\omega' = \frac{I_1}{I_1 + I_2}\omega_0 \tag{8}$$

Also, Eq. 7 becomes as follows;

$$T_{f0}\theta_2 = \frac{I_1^2\omega_0^2}{2(I_1 + I_2)} \tag{9}$$

Eq. 9 shows the law of energy conservation, as the left side is the amount of work in one cycle and the right side is the kinetic energy of the body and wheel right after the connection of the clutch. Also, the dispassion of kinetic energy ΔE caused by the clutch connection is as follows;

$$\Delta E = \frac{I_1\omega_0^2}{2} - \frac{I_1^2\omega_0^2}{2(I_1 + I_2)} = \left(\frac{I_2}{I_1 + I_2}\right)\frac{I_1\omega_0^2}{2} \tag{10}$$

As ΔE causes strong mechanical shock stress, the mechanism must be designed to bear this stress.

3. PROTOTYPES AND EXPERIMENTS

We report on three prototypes and their experimental results, namely Prototypes 1, 1A and 2.

3.1. Prototype 1

3.1.1 Concept

The first prototype (Prototype 1) is used to demonstrate the basic STSM concept, which consists of minimal parts.

3.1.2 Design

Fig. 6 shows a schematic drawing and photograph of Prototype 1, with its specification indicated in Tab. 1.

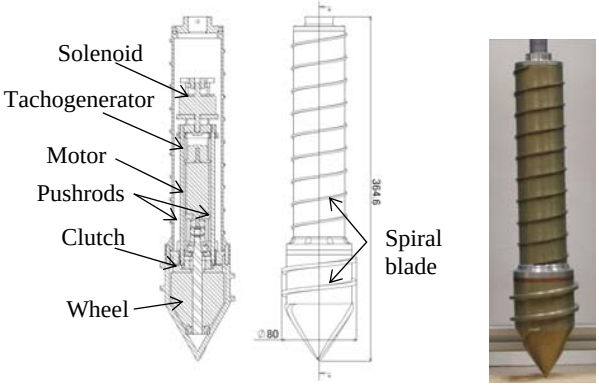

Figure 6. Schematic drawing and picture of Prototype 1 of STSM

Table 1. Specification of Prototype 1

Rotate with the wheel	weight [kg]	1.07
	MOI I_1 [kgm^2]	3.83×10^{-4}
Rotate with the body	weight [kg]	1.40
	MOI I_2 [kgm^2]	7.12×10^{-4}
Motor	manufacture, type	Maxon, RE25
	power [W]	20
Solenoid	manufacture, type	Shindengen, 4EC
	power [W]	100

Prototype 1 is 364.6 mm in length, 80 mm in diameter, and weighs about 2.5 kg. The cylindrical body and spiral blade on the outer surface of the body are machined from a bulk of aluminum alloy and the screw pitch is 24 mm. The outer surface of the body is coated in polytetrafluoroethylene (or PTFE) to reduce the friction acting between the body and regolith. The brass-made wheel is supported by two rotational bearings inside the body, and the wheel and shaft of the motor are mechanically coupled. The motor housing is fixed to the body. The angular velocity of the motor is monitored by a tachogenerator attached to the motor, while the solenoid drives the clutch via the pushrods.

Fig. 7 shows the clutch motion. Tooth 1 rotates with the body and is able to slide along its axis. When the solenoid is not activated, tooth 1 is in a stored position due to the retaining force of the return spring (Fig. 7 (1)). When the solenoid is activated, tooth 1 is pushed by the pushrods and engages with tooth 2 (Fig. 7 (2)). To reduce the wear of these teeth, they are made from SCM415 steel and heat-treated.

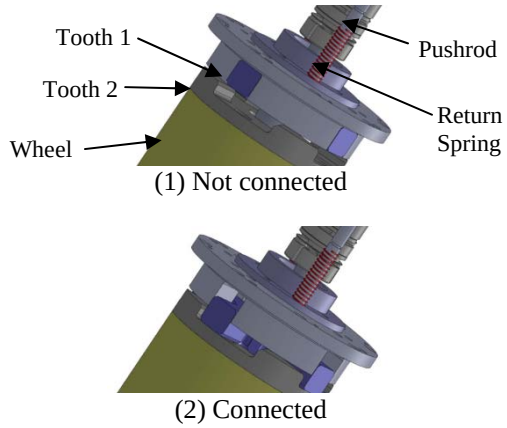

Figure 7. Clutch Mechanism of Prototype 1

3.1.3 Experiment

Fig. 8 shows a block diagram of the whole system used for the experiment.

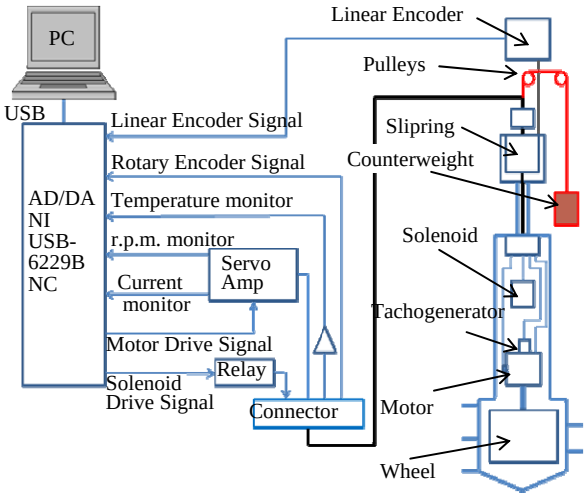

Figure 8. Diagram of the experiment system

We used DAQ (National Instruments USB-6229BNC) to control the hardware. The servo amp for motor control is Maxon ADS50/5, and the solenoid is controlled via a mechanical relay. The angular velocity of the motor, electric current to the motor and motor and solenoid temperatures are monitored. To avoid the motor and solenoid overheating, the operation is to be halted when the temperature exceeds the threshold value.
Fig. 9 shows the setup of the experiment. The blue cylinder located in the lower part of the picture is a steel drum (inner diameter is 567 mm and inner height is 830 mm), which contains fly ash to simulate the lunar regolith. Fly ash is one of the residues generated in combustion, and comprises fine particles that rise with flue gases, with characteristics similar to lunar regolith as shown in Tab. 2.
An aluminum frame support structure prevents the STSM from falling down initially, but does not support reactive torque for excavation. An aluminum pipe of 20 mm diameter is connected to the tail part of the STSM, through which wires for power and signals are routed. To prevent twisting of the wires as the body rotates, a slipring is attached to the top of the connecting pipe. Rotation of the body and its depth of penetration are measured by a rotary encoder (Mutoh Engineering MH-600) and a linear encoder (Mutoh Engineering D-1000Z), respectively.

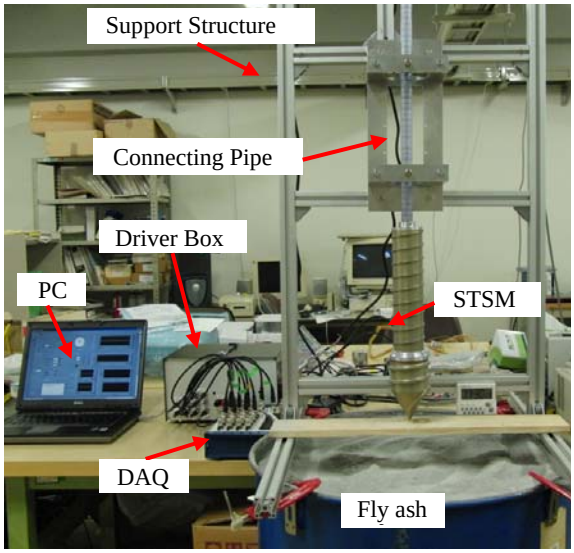

Fig. 9 Experimental system

Table 2. Comparison of lunar regolith and flyash

	Lunar Regolith	Fly ash (JIS class 5)
Density [g/cm^3]	1.45~1.79 [6]	1.2~1.6
Median grain size [μm]	42~802 [6]	13~17 [8]
Cohesion *c*[kPa]	0.1~1 [7]	0.57 [9]
Friction Angle ϕ[degrees]	30~50 [7]	33.8 (=tan^{-1} 0.67) [9]

The STSM was connected to the counterweight (5/6 of the STSM weight) by a steel wire to simulate weight on bit (WOB) on the Moon. The gravitational force acting on the body aids its downward penetration, but that exerted on the regolith disturbs excavation. Accordingly, the condition of this experiment is supposed to be more severe than that on the Moon.

3.1.4 Results

We proceeded to conduct experiments 4 times with Prototype 1. During these experiments, the maximum rotational speed of the wheel was about 1200rpm, and one cycle lasted about 4 seconds. Experiment No. 1 was without a counterweight and Nos. 2 to 4 included it.
Fig. 10 shows the measured depth of penetration during the experiments. The horizontal axis indicates the number of cycles and the vertical axis is the depth of penetration. When the tip of the body touches the surface of the fly ash, the depth is 0 mm. In experiment No. 3, it was shown that the STSM has the ability to

reverse to eject itself from the fly ash. In experiment No. 4, meanwhile, the depth of penetration reached 669 mm at 12910 cycles. All the experiments except No. 3 were aborted due to failures of the mechanism, such as breaking of the electrical wire or mechanical parts. These failures seem attributable to the repeated mechanical shocks transmitted from the clutch, hence the need to reduce such shock transmission.

The inclination of the graph of Fig. 10 shows the rate of penetration (ROP). As is clear, the ROP of the experiments varies widely, which we presume to be attributable to the variation in hardness of the fly ash, making it important to measure and adjust the hardness of the same.

Fig. 11 shows the scenery of experiment No. 3. During this experiment, the reverse drive started at 3 hours, and Prototype 1 finally came out of the regolith.

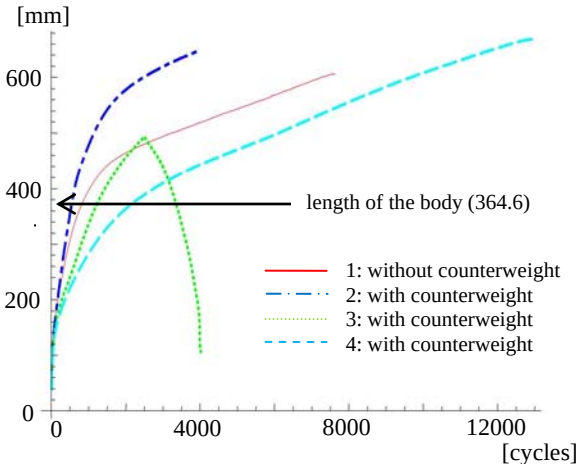

Figure 10. Depth of Penetration

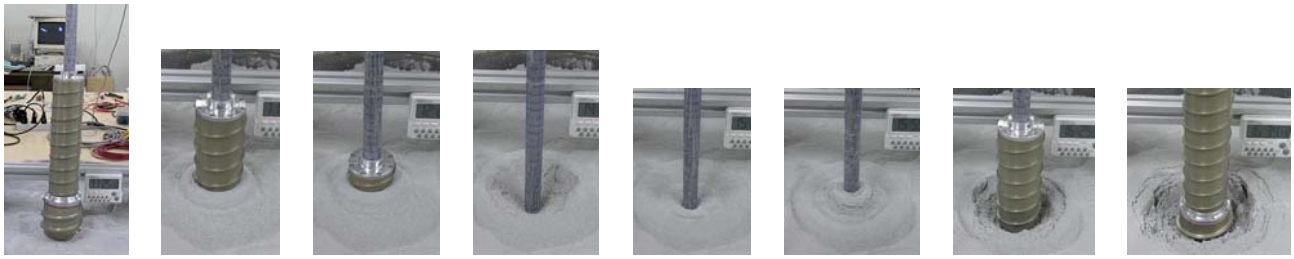

(1) 0 min. 0 cycle | (2) 30 min. 391 cycles | (3) 1 hr. 780 cycles | (5) 3 hr. 2335 cycles | (6) 4 hr. 3091 cycle | (7) 4 hr. 30min. 3480 cycles | (8) 5 hr. 3869 cycles | (9) 5 hr. 9 min. 3988 cycles

Figure 11. Experiment no.3 of Prototype 1(with counter-weight)

3.2. Prototype 1A

Through the experiment of Prototype 1, it became clear that the mechanical shock transmitted from the clutch might result in failure of the payload or the mechanism itself. Accordingly, we introduced a floating inner frame concept to reduce the transmission of mechanical shock to the payload and mechanisms (Fig. 12).

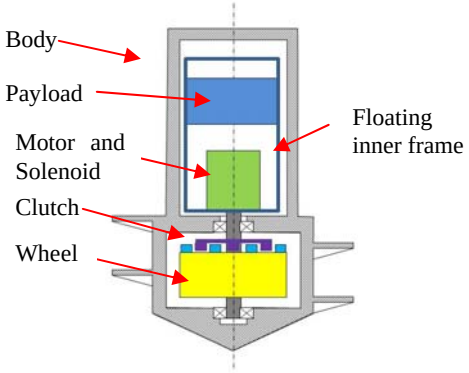

Figure 12. Conceptual view of STSM with floating inner frame

The floating inner frame is supported by rotational bearings in the body and is freely rotatable about its axis. The motor, clutch and payload are attached to the floating inner frame. When the clutch is engaged, the body starts to rotate, but the floating inner frame remains still, meaning the transmission of mechanical shock is significantly reduced.

In addition, this concept has the following features:

(i) Eliminates the need for a slipring, because all the electrical wires are connected to parts fixed to the non-rotating floating inner frame;

(ii) The amount of work in one cycle increases because I_2 in Eq. 7 is reduced;

(iii) The axis of rotation of the floating inner frame can be used as the axis of a gimbals mechanism, as described later in 3.3.2.

3.2.1. Design

To demonstrate the concept of the floating inner frame, we modified Prototype 1 and named it Prototype 1A (Fig. 13). It includes the floating inner frame inside the body, which is supported by two rotational bearings and to which the motor and solenoid are fixed.

The connecting mechanism between the tooth and solenoid must transmit the axial movement of the solenoid and accept rotational movement between the body and the floating inner frame. Fig. 14 shows the motion of the clutch. Tooth 1 rotates with the body and is able to slide along its axis. When the solenoid is not activated, tooth 1 remains in the stored position via the

retaining force of the return spring fixed to the body (Fig. 14(1)). When the solenoid is activated, pushrod 1 pushes the pushring, which pushes pushrod 2, which, in turn, pushes tooth 1, meaning tooth 1 is engaged with tooth 2 (Fig. 14(2)). As pushrod 1 and the pushring are not fixed to each other, the rotational movement between the body and floating inner frame is accepted.

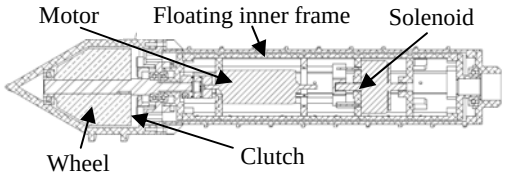

Figure 13. Schematic drawing of Prototype 1A

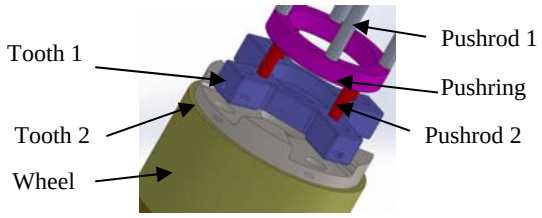

(1) Not connected

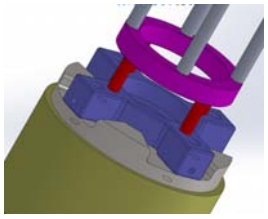

(2) Connected

Figure 14. Clutch Mechanism of Prototype 1A

Tab. 3 shows a comparison of the MOI of the prototypes. Based on Eq. 9, the rotation angle of one cycle is proportional to $I_1^2/(I_1+ I_2)$, meaning Prototype 1A is expected to rotate 16% more than Prototype 1 under the same condition.

3.2.2. Results

Fig. 15 shows the depth of penetration of Prototypes 1 and 1A. Prototype 1A penetrated 724 mm at 9464 cycles, while the deepest record of Prototype 1 is 669 mm at 12910 cycles. It is clear that Prototype 1A performed better than Prototype 1. However, the performance improvement cannot be conclusively confirmed, because the soil hardness of the fly ash may differ in each experiment.

Fig. 21 is the shock response spectrum (SRS) of acceleration which is measured inside prototypes. The acceleration level of Prototype 1A is much less than that of Prototype 1, proving how the floating inner frame reduces the transmission of mechanical shock.

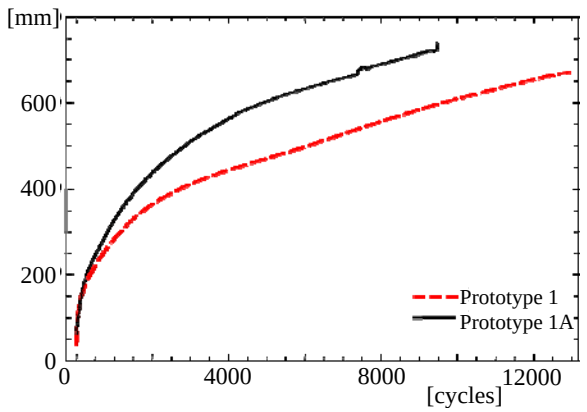

Figure 15. Depth of Penetration of Prototype 1 and 1A

3.3. Prototype 2

3.3.1. Concept

We designed Prototype 2 to demonstrate that STSM has the ability to carry sufficient payload. The dimensions of Prototype 2 exceed those of its predecessors, but it uses the same motor and solenoid and thus has equivalent power consumption.

3.3.2. Design

Prototype 2 is designed to carry two types of mass dummies, namely A and B respectively. Mass dummy A resembles the seismometer for the LUNAR-A penetrator [5], which is 50 mm in both diameter and length. The mass dummy A is installed with a gimbals mechanism, as the LUNAR-A penetrator has strict leveling requirements. The floating inner frame can rotate about the axis of the body, so we used this axis as one of the axes of the gimbals mechanism. The mass dummy B is 50 mm in diameter and 100 mm in length, but does not resemble any existing sensors.

Figs. 16 and 17 show the final Prototype 2 design, which is 632 mm in length and 120 mm in diameter, with a screw pitch of 36 mm. The cylindrical body and spiral blade are machined from a bulk of aluminum alloy. The outer surface of the body is coated in PTFE.

The casing of the motor is fixed to the floating inner frame and placed inside the wheel to shorten the total length of the mechanism. The solenoid and mass dummies are fixed to the floating inner frame. The solenoid and clutch are connected with a similar mechanism to Prototype 1A. As you can see in Tab. 3, I_1 of Prototype 2 is more than 10 times the others.

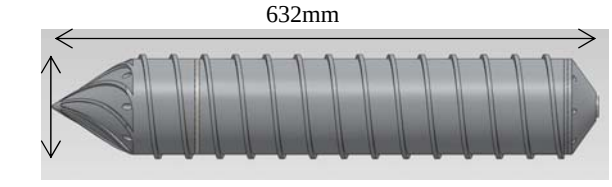

Figure 16. Prototype 2

As all prototypes use the same motor and solenoid, we can use the same control system although Prototype 2 requires longer for wheel acceleration.

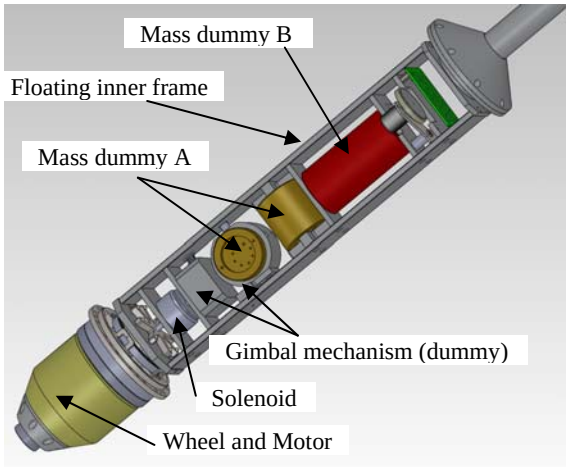

Figure 17. Inside of Prototype 2

Table 3. Comparison of moment of inertia (MOI) (x10^{-4} kgm^2)

	I_1	I_2	I_3	$I_1^2/(I_1+I_2)$
prototype 1	3.83	7.12	-	1.34
prototype 1A	3.87	5.74	1.52	1.56
Prototype 2	42.8	57.9	18.5	18.2

3.3.3. Experiments

Fig. 18 shows the experimental setup of Prototype 2. As the weight of Prototype 2 is 11.6 kg, we used a counterweight of 9.7 kg to simulate WOB on the Moon. During the penetration experiment, the wheel acceleration time and maximum wheel rotation speed were adjusted for Prototype 2. Cycle time was about 10 seconds and clutch connection occurred at a wheel rotational speed of about 500 r.p.m. We used the same control system and software as Prototype 1 and 1A.

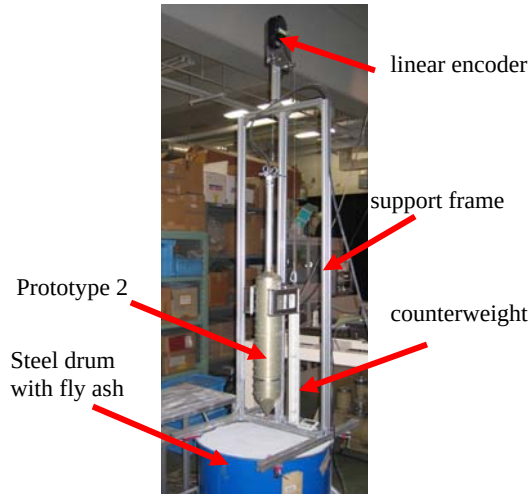

Figure 18. Experimental setup of Prototype 2

3.3.4. Results

Fig. 19 shows experimental scenery of Prototype 2. Captions under pictures indicate time and cycles. Fig. 20 shows its depth of penetration. It reached the bottom of the steel drum (depth = 812.6 mm) at 8175 cycles, whereupon we started to drive backward and most of the body was ejected from fly ash at 10774 cycles.

It took 24h33m39s to penetrate 710 mm (initial penetration was 102 mm), equating to an average penetration rate of 28.9 mm/h.

We measured the mechanical shock acceleration near mass dummy A. The SRS of Prototype 2 is much reduced compared to Prototype 1 and 1A, as shown in Fig. 21. We presume this to be attributable to the wheel rotational speed of Prototype 2 being 500 r.p.m., as compared to about 1000 r.p.m. for the others, while the inner frame of Prototype 2 is far heavier and stiffer than that of Prototype 1A.

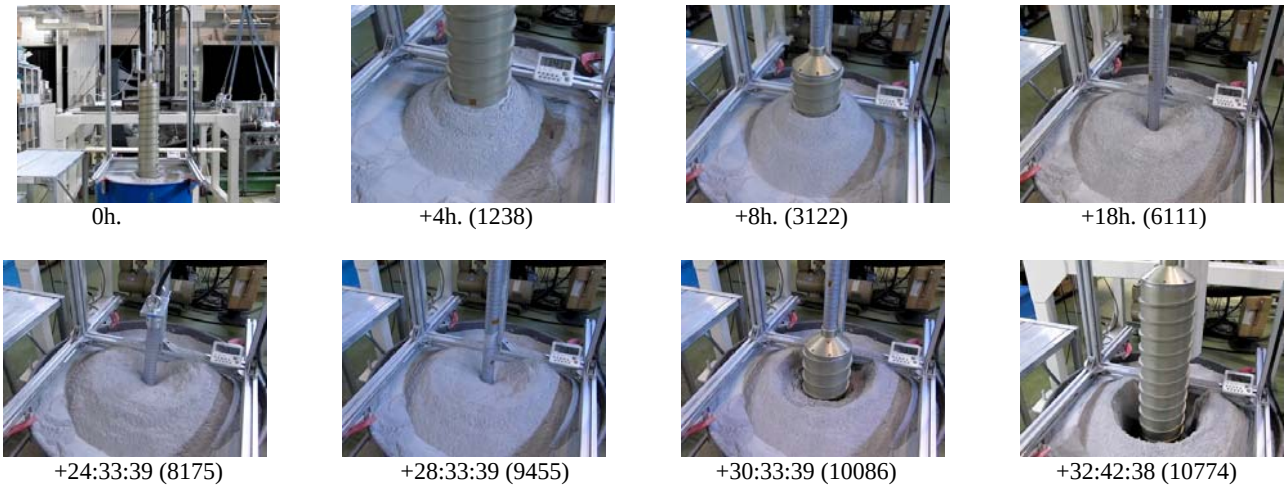

Figure 19. Experimental scenery of Prototype 2

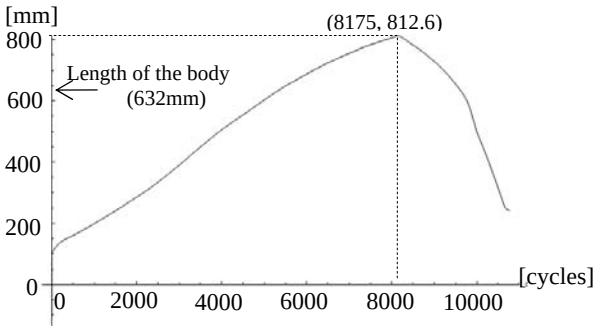

Figure 20. Depth of Penetration of Prototype 2

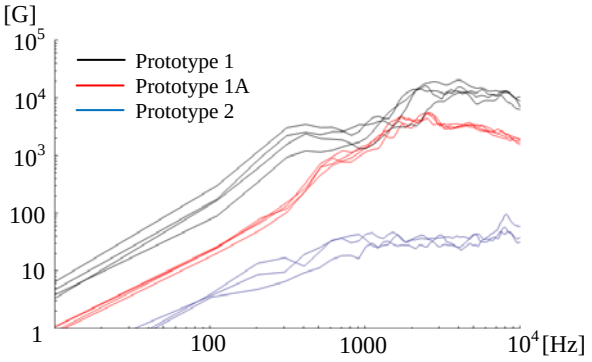

Figure 21. Shock Response Spectrum of acceleration

4. CONCLUTION AND FUTURE WORKS

We proposed a novel mechanism named the 'Self-Turning Screw Mechanism' (STSM) via which to install geophysical sensors under the regolith. We built some prototypes and demonstrated its feasibility and capability to carry some payload. STSM also includes several preferable features for unmanned lunar/planetary exploration.

To develop unmanned lunar/planetary environment sensing systems, some other mechanisms such as supporting mechanisms, tether winching mechanisms, power supply systems and an interface mechanism for lunar landers/rovers must all be developed.

ACKNOWLEDGEMENTS

We would like to give thanks to Dr. H. Shiraishi in JAXA, Mr. Y. Horikawa in University of Tokyo and Dr. K. Nagaoka in Tohoku University for supporting our experiments. Also, discussions with them have been illuminating.

References

1. Hashimoto, T., Tanaka, S., Hoshino, T., Otake, H. & Otsuki, M. (2011). Recent Study Progress on A Lunar Landing Mission SELENE-2. In *Proc. of the 28th ISTS, 'International Symposium on Space Technology and Science'*, Okinawa, Japan, 2011-k-07.
2. Watanabe, K., Shimoda, S., Kubota, T. & Nakanishi, I. (2003). A Mole-Type Drilling Robot for Lunar Subsurface Exploration. In *Proc. of the 7th i-SAIRAS 'International Symposium on Artificial Intelligence and Robotics & Automation in Space'*, Nara, Japan, AS-7.
3. Gorevan, S. P. & etal. (2001). An inchworm deep drilling system for kilometer scale subsurface exploration of mars (IDDS). *Innovative Approaches to Outer Planetary Exploration 2001–2020*, p.68.
4. Yasuda, S. (2011). Autonomous excavating apparatus. *United States Patent*, 8061441.
5. Yamada, R., Yamada, I., Kobayashi, N., Takeuchi, N., Shiraishi, H., Tanaka, S., Fujimura, A., Mizutani, H. (2005). Characteristics of a seismometer for the LUNAR-A penetrator., In *Proc. of 36th Lunar and Planetary Science*, Houston, TX, USA, #1715.
6. Heiken, G., Vaniman, D., French, B. (1991). *Lunar sourcebook*, Cambridge University Press, Cambridge, UK, p.305.
7. Heiken, G., Vaniman, D., French, B. (1991). *Lunar sourcebook*, Cambridge University Press, Cambridge, UK, p.506.
8. The Association of Powder Process Industry and Engineering JAPAN, *JIS test powders 1 classification and characteristics*, Online at http://appie.or.jp/testpowders_e/class/index (As of 31 May 2012).
9. Yoshida, K., Kudo, H., Kawakatsu, Y., Yokoyama T., Sonoyama, M. (2000). Development of a Mole-like Robot for Lunar Subsurface Exploration [In Japanese], In Proc. of *ROBOMEC2000 'JSME Robotics and Mechatronics Conference 2000'*, Kumamoto, JAPAN, 1P1-07-019.